



## Research Paper

**Cite this article:** Iqbal J, Illahi U, Ramay SM, Sulaiman MI (2024) Circularly polarized dual-port MIMO DRA for future Wi-Fi 6E applications. *International Journal of Microwave and Wireless Technologies*, 1–12. <https://doi.org/10.1017/S1759078724000576>

Received: 9 January 2024

Revised: 29 April 2024

Accepted: 13 May 2024


### Keywords:

circular polarization; DRA; MIMO; WiFi 6E application

**Corresponding author:** Javed Iqbal;

Email: [Javediqbal.iet@gu.edu.pk](mailto:Javediqbal.iet@gu.edu.pk)

# Circularly polarized dual-port MIMO DRA for future Wi-Fi 6E applications

Javed Iqbal<sup>1</sup> , Usman Illahi<sup>1</sup>, Shahid Mahmood Ramay<sup>2</sup> and Mohamad Ismail Sulaiman<sup>3</sup>

<sup>1</sup>Electrical Engineering Department, Gomal University, Dera Ismail Khan, KPK, Pakistan; <sup>2</sup>Physics and Astronomy Department, College of Science, King Saud University, Riyadh, Kingdom of Saudi Arabia and <sup>3</sup>Science Team, University of Sheffield International College, Sheffield, United Kingdom

## Abstract

This research article proposes a dual-sense dual-port wideband circularly polarized (CP) multi-input multi-output (MIMO) antenna designed for Wi-Fi 6E applications. The main novelty lies in achieving CP for both ports using a truncated rectangular-shaped aperture. By incorporating design and spatial diversity and defective ground structure between the two radiators, the design improves isolation and enables the antenna to generate Left-Hand Circular Polarization (LHCP) depending on the selected feed port. The proposed MIMO rectangular dielectric resonator antenna demonstrates an impressive impedance-matching bandwidth (IBW) from 5.5 to 8.0 GHz (37.10%) as well as an axial ratio bandwidth (ARBW) covering from 6.0 to 6.55 GHz (12.20%). Additionally, the dual-port wideband CP MIMO antenna exhibits satisfactory diversity performance parameters. To validate the simulated results, a physical prototype is fabricated and subjected to experimental testing. The measured outcomes of the fabricated model align closely with the simulated results, confirming the accuracy of the design. With both MIMO and CP capabilities and improved isolation, this proposed model proves beneficial in reducing latency and minimizing the impact of multipath fading. Therefore, it stands as an excellent choice for future devices utilizing the Wi-Fi 6E band due to its broad IBW and overlapping AR.

## Introduction

The most common form of communication for gadgets that require internet connectivity for their extended operation is Wi-Fi. Encompassed within are essential communications for missions, which involve the Internet of things, cellular gadgets having enhanced bandwidth, and other related technologies. Wi-Fi utilizes the quadrature amplitude modulation (QAM) technique, with Wi-Fi 5 employing the 512-QAM method, enabling devices to broadcast 8 bits concurrently. In Wi-Fi 6, 1024-QAM is employed to boost speed and ultimately the bits transmission rate. As a result, 10 bits can now be delivered simultaneously at a faster rate. That assists in an additional 25% in speed. Wi-Fi not only enhances the performance of smart devices but also enables the use of virtual reality and augmented reality apps. The ability to remotely manage machinery, medical operations, crucial infrastructure, and vehicles is made possible by low latency and ultra-reliable networks in the industry [1]. Higher data rates and bandwidth are required due to the rise in demand for these applications. A simple solution like multi-input multi-output (MIMO) can meet the needs because of limited bandwidth resources and high data rate demands.

MIMO technology has demonstrated its ability to improve data rates, communication quality, and bandwidth while keeping power consumption unchanged. The performance of MIMO systems heavily relies on the design and configuration of antennas, which are essential for mitigating the effects of multipath propagation in wireless channels [2, 3]. However, the research literature has relatively few articles discussing MIMO dielectric resonator antennas (DRAs), indicating they might not be as extensively explored as other antenna types. In one study [4], an MIMO rectangular DRA (RDRA) was proposed for 4G applications, but its fabrication process proved to be intricate due to the incorporation of a shorting pin and metallic strip.

Another research work [5] introduced a cylindrical DRA for MIMO applications, which improved port isolation through the use of slits in the ground plane. However, the insertion of the cylindrical DRA into an FR4 substrate added complexity to the fabrication process. Overall, there are limited reports in the literature on dual-port MIMO antennas with circular polarization (CP) covering the Wi-Fi 6E band and having narrow impedance-matching bandwidth (IBW) and axial ratio bandwidth (ARBW). Recently, CP radiators have gained significant attention among antenna designers for MIMO systems [6]. Although both CP and linearly polarized antennas emit radiation, CP antennas offer advantages in

© The Author(s), 2024. Published by Cambridge University Press in association with The European Microwave Association. This is an Open Access article, distributed under the terms of the Creative Commons Attribution licence (<http://creativecommons.org/licenses/by/4.0>), which permits unrestricted re-use, distribution and reproduction, provided the original article is properly cited.

mitigating the negative effects of multipath. They are less sensitive to the orientation of transmitter (Tx) and receiver (Rx) antennas, making them well-suited for wireless networks [7] and transceiver applications [8].

Moreover, they create a dependable connection between the transmitting and receiving systems, regardless of their orientation. Ref. [9] highlights that utilizing CP radiators in MIMO antenna systems can be a promising approach for both indoor and outdoor scenarios, offering several advantages over linearly polarized radiators.

Researchers have introduced various CP MIMO antennas with two-port [10–13] and four-port [14–16] configurations. Among these, a four-port CP antenna with a planar structure and DRA has been proposed [17, 18]. In smart Wi-Fi devices, the planar and DRA shape is highly preferred for accommodating the antennae. However, none of the existing antennas were discovered to resonate at the Wi-Fi 6E band (5.90–7.10 GHz), and the four-port configuration failed to meet the user requirements. Another study [19] introduced a CP dual-band MIMO antenna with a multi-layer structure, which exhibited decent antenna performance in a higher frequency band. However, it was considered unsuitable for the intended Wi-Fi 6E application range due to the overlapping axial ratio (AR) and IBWs.

Additionally, in papers [20, 21], planar CP MIMO antennas were proposed with center frequencies of 3.6 GHz and 2.44 GHz, IBWs of 11.11% and 3.27%, and ARBs of 13.88% and 40.34%, respectively. Nevertheless, even with DRA geometry and respectable antenna properties, these operational bands still necessitate a dual-port CP antenna resonating in the Wi-Fi 6E spectrum.

This paper introduces a miniature, dual-element, two-port, double-sense RDRA tailored for MIMO applications. The RDRA design incorporates truncated rectangular-shaped apertures to generate CP waves. Specifically, one port of the aperture produces LHCP waves, while the other port generates Right-Hand Circular Polarization (RHCP) waves. This arrangement achieves an impressive overlapping bandwidth, covering both IBW and AR at 20.20%. The adoption of a carefully chosen defective ground geometry contributes to a favorably improved isolation and wide IBW characteristic. To assess the MIMO performance, the paper evaluates the envelope correlation coefficient (ECC) parameter. The findings suggest that the MIMO antenna design holds promising potential for future Wi-Fi 6E wireless applications, owing to its DRA configuration and the ability to achieve circular polarization without the need for a complicated process.

## Antenna design and analysis

### Single element antenna

Figure 1(a) illustrates the three-dimensional model of the single-element antenna positioned on a  $25 \times 25$  mm ( $L \times W$ ) ground plane with a substrate height ( $H_s$ ) of 1.6 mm. The optimal dimensions of the RDRA and periodic truncated rectangular-shaped apertures are detailed in Table 1. Further elaboration on the dielectric material, substrate, and feeding mechanism is provided in the subsequent section.

Utilizing periodic truncated rectangular-shaped apertures is a technique employed to generate CP [22], which aligns with the objectives of this research. Fundamentally, the square ring functions as a network to induce sequential phase shifts of  $0^\circ$ ,  $90^\circ$ ,  $180^\circ$ , and  $270^\circ$  at the four edges of the loop. This phenomenon facilitates

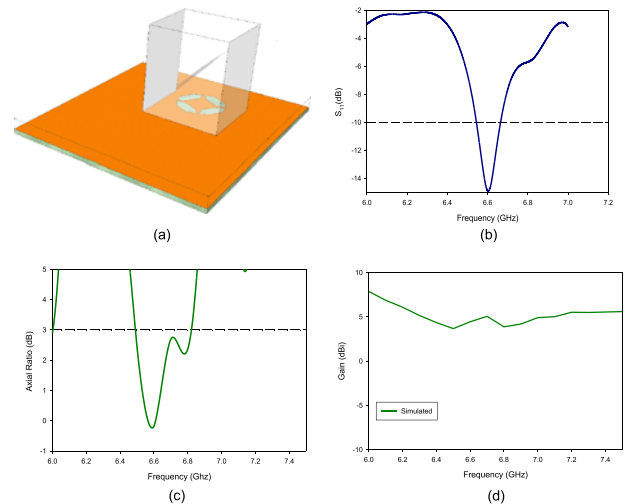


**Figure 1.** Schematic diagram of the single element antenna: (a) 3D-design; (b) reflection coefficient; (c) axial ratio; and (d) gain.

**Table 1.** Augmented dimension of the projected wide band CP MIMO antenna

Elements	Parameters	Dimensions (mm)
Length ground/substrate	$L_S, L_G$	53, 53
Width ground/substrate	$W_S, W_G$	53, 53
Height of substrate	$H_S$	1.6
RDRA	$H, W, D$	26, 25, 20
Distance between DRs	$D_R$	13
Truncated rectangular-shaped apertures width, breadth, and gap, arc	$W_p, B_p, D, \Theta$	4, 2, 1, $90^\circ$
DGPS, arc	$H_1, H_2, \Theta$	2.5, 25, $80^\circ$
Microstrip feed (length/width)	$H_S/W_S$	30, 3

the attainment of the desired response critical for generating the CP field and maintaining the phase difference between the generated orthogonal modes.

Observably, two orthogonal degenerate modes manifest at 6.6 GHz and 6.8 GHz, contributing to CP generation at a frequency of 6.6 GHz. The single antenna exhibits an IBW of 8.43% (6.54–6.6 GHz), as depicted in Figure 1(b), alongside a 3 dB AR passband extending from 6.48 to 6.82 GHz, offering a 12.9% ARBW, as shown in Figure 1(c). Conversely, Figure 1(d) illustrates the average gain of the single element, maintaining a nearly 5 dBi level throughout the desired band.

### Proposed MIMO antenna

Figure 2 illustrates the suggested configuration of the CP MIMO RDRA. The primary emphasis lies on the feeding mechanism and its three-dimensional depiction. Figure 2(a) depicts the complete proposed 3D model. While Figure 2(b) shows the backside view which comprises a standard microstrip feed line. However, the feed line has undergone meticulous optimization to achieve a  $50 \Omega$  impedance matching. The main part of the proposed design,

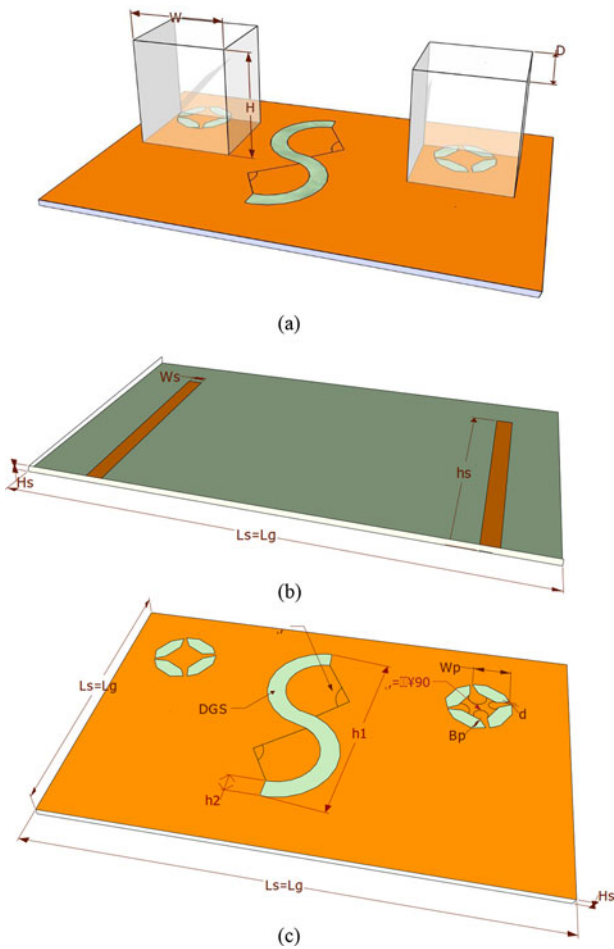


**Figure 2.** Schematic diagram of the proposed wideband CP MIMO antenna: (a) proposed design, (b) feeding structure, back side of the ground; and (c) DGS/truncated rectangular-shaped apertures 3D view.

i.e., defected ground structure (DGS) and truncated rectangular-shaped aperture is illustrated in Figure 2(c). The etched structure on the ground plane plays a pivotal role in generating a CP wave-form directed broadside.

Two symmetrically arranged truncated rectangular-shaped apertures are employed at ports 1 and 2. To improve isolation, S-shaped DGS slits are incorporated into the upper portion of the ground plane between the two feeding ports. For the antenna simulation and optimization, the CST MWS tool is utilized. The antenna's compact dimensions in its basic form are  $53 \times 53 \times 1.6$  mm, and it is built using an FR-4 substrate with a dielectric constant ( $\epsilon_r$ ) of 4.4 and a loss tangent ( $\tan \delta$ ) of 0.02. The optimized antenna dimensions can be found in Table 1.

**Design evolution steps**

This section presents a discussion of the simulated design evolution and its corresponding steps. Figure 3 depicts the iterative progression from the basic RDRA design to the proposed design. To get the optimum dimension, a comprehensive parametric study has been performed using an finite element method (FEM)-based simulation tool. A pair of simple RDRA are placed on the ground plane. Both the DR elements are tightly spaced with an optimum

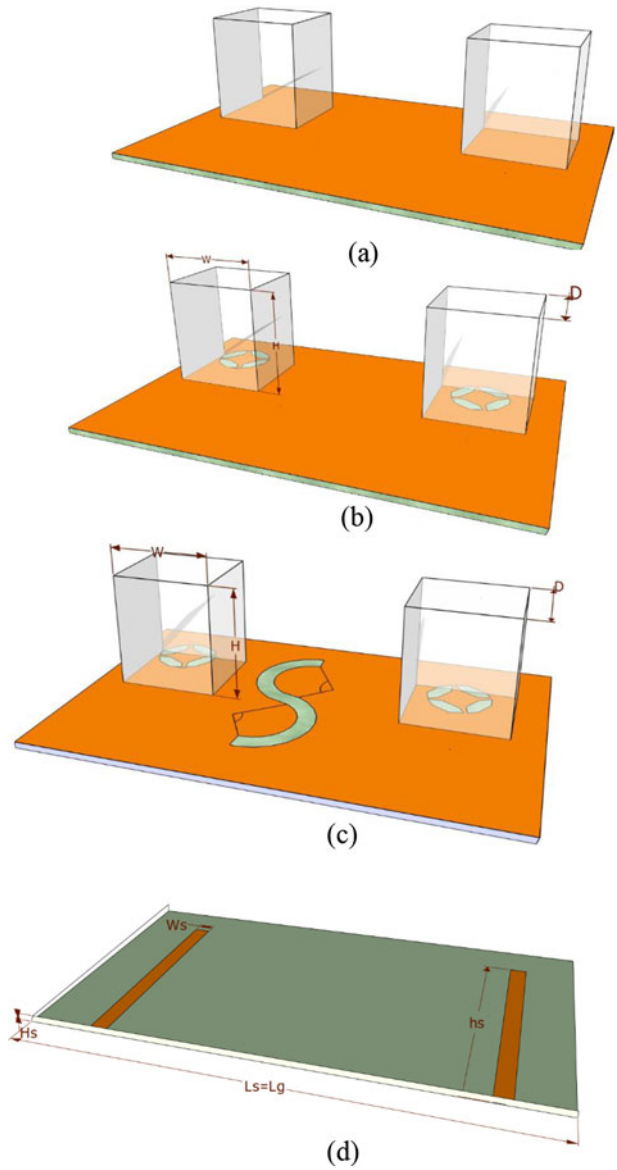


**Figure 3.** Evolution of the 3D view of the RDRA, (a) a basic RDRA pair. (b) Truncated rectangular-shaped apertures base RDRA. (c) Proposed design (DGS). (d) Backside view of microstrip lines.

gap after running the intense simulations. In order to reduce surface wave current, the substrate of a low permittivity of around 4.4 is used. It consists of an alumina ceramic-based rectangular dielectric resonator (DR) ( $\epsilon_r = 9.8, \tan \delta = 0.02$ ) placed over an FR-4 substrate ( $\epsilon_{sub} = 4.4, \tan \delta = 0.02$ ), resulting in an overall size of  $53 \times 53 \times 1.6$  mm<sup>3</sup>. The ECCOSTOCK HiK material has been utilized to create RDRAs having a permittivity of 9.8 shown in Figure 3(a). For the generation of CP waves, two modified rectangular corner truncated-shaped apertures have been etched. Both are mirror images of one another as described in Figure 3(b), used at port 1 and port 2. Figure 3(c) and (d) illustrates the 3D view of the proposed model from the top and backside respectively.

**Simulated results**

The proposed two-port wideband CP MIMO antenna adopts the elementary antenna's geometry. The ground plane has been

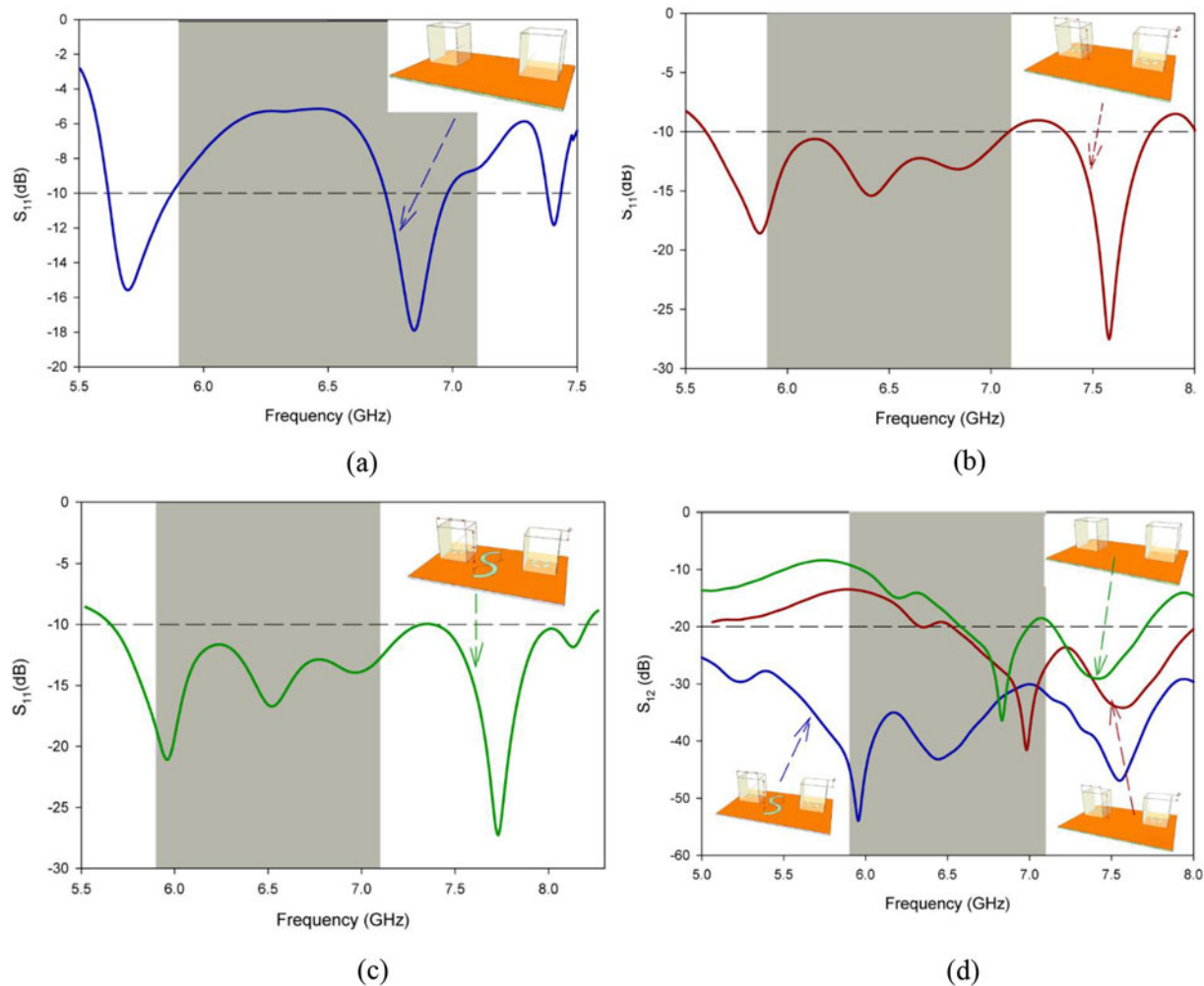


**Figure 4.** S-parameter parametric analysis results of all three antennas: (a)  $S_{11}$  antenna (a), (b)  $S_{11}$  antenna (b), (c)  $S_{11}$  antenna (c), and (d) isolation  $S_{21}$ .

modified with truncated rectangular-shaped apertures etched on the upper side, and a simple microstrip line is employed on the lower part of the ground plane. Port 1 and port 2 incorporate two modified rectangular corner truncated-shaped apertures, which act as symmetrical mirror images of one another. To improve isolation, S-DGS slits are etched between the two feeding ports on the upper section of the ground plane. Even though a shared ground geometry is commonly suggested for MIMO configurations [36], it is not used in this particular case. This decision stems from the fact that the CP performance is highly dependent on the ground plane geometry.

Connecting the antenna to a common ground would adversely affect the performance. As a result, the current MIMO antenna employs a separate ground plane structure to effectively maintain its CP performance. Figure 4 presents the simulated reflection coefficient  $S_{11}$  and transmission coefficient  $S_{12}$  for all three stages of the MIMO antenna. The simulated  $S_{11}$  performance of the integrated antenna is illustrated in Figure 4(a). It is basically a dual-band antenna, it can be seen that  $|S_{11}| \leq 10$  dB frequency bands are obtained with one centered at 2.02 GHz and the other at 5.7 GHz. The bandwidths of the two operational bands are 5.6–5.88 GHz (4.87%) and 6.73–7.0 GHz (4.0%), respectively.

The antenna 3(a) provides a narrow bandwidth in the desired band (5.9–7.1 GHz). The antenna 3(b) exhibits dual-band characteristics too, an impressive IBW spanning 24.54% (from 5.6 to

7.1 GHz) and 5.5% from 7.36 to 7.78 GHz covering the whole desired band in addition to this an ARBW of 20.20% (from 5.58 to 6.69 GHz) has been attained as depicted in Figure 3(b). Upon close examination of Figure 3(c), it is evident that the reflection coefficients  $S_{11}$  for both antenna 3(b) and (c) are nearly identical, except for antenna 3(a). The broadened response observed in antennas 3(b) and (c) is attributed to the synergistic influence of two pivotal factors: cavities and resonance [22]. A novel design methodology is introduced herein, entailing the arrangement of sequential patches periodically. These patches, characterized by truncated rectangular-shaped apertures, are strategically positioned on the substrate (ground plane) to augment the impedance-matching bandwidths.

As we know, cavities play an important role in IBW enhancement by etching on the ground plane, e.g., resonant cavity antenna. Moreover, these truncated apertures are placed in a periodic manner to generate the resonance, and by converting a single element into MIMO the overall resonance increases, the presence of multiple resonances can lead to a wider impedance-matching bandwidth compared to a single resonance. This is because each resonance point contributes to the overall bandwidth of the antenna. These multiple resonant modes are simultaneously excited to broaden the bandwidth of a proposed antenna by about 32%. Several resonant modes are clearly visible in Figure 4(b) and (c), same concept has been used in [37]. Conversely, in Figure 3(a), the absence

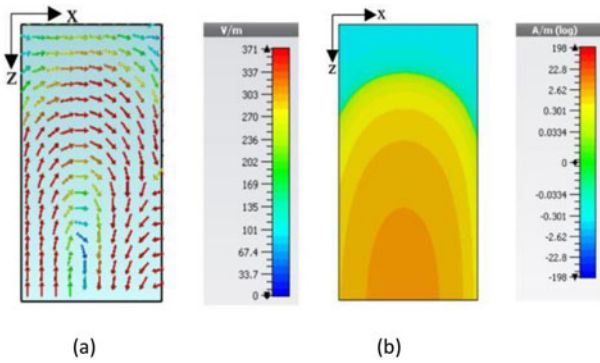


**Figure 5.** Linearly polarized RDAR field distribution of  $TE_{1\delta 1}^y$  at 6.84 GHz. (a) E-field and (b) H-field.

of truncated rectangular-shaped apertures results in a narrower impedance-matching bandwidth performance, as illustrated in Figure 4(a).

However, the transmission coefficients  $S_{21}$  show considerable differences. At the resonant frequency of 6.8 GHz, Figure 3 exhibits  $S_{21}$  at approximately  $-20$  dB, while Figure 3(b) records  $-23$  dB. Figure 3(c) stands out with a significantly reduced mutual coupling (MC), reaching approximately  $-46$  dB, as shown in Figure 4(d).

The observed results can be attributed to the polarization properties of the two DRAs used in Figure 3(b). Both antennas exhibit the same polarization characteristics in this arrangement, generating LHCP waves upon excitation. As a result, a significant level of MC between the two DRAs is observed. On the other hand, Figure 3(c) takes advantage of the S-shaped DGS implementation, leading to a noteworthy reduction in MC. The working principle of the DGS will be explored in more detail later. Similarly, when two CP antennas are positioned adjacently, the mutual interference is relatively faint [23], which corroborates the findings of this investigation.

On the other side, Figure 3(a) only excites the single fundamental mode  $TE_{1\delta 1}^y$  inside the DRA, which is evident from the E and H-field as depicted in Figure 5. The AR is not shown here because the Figure 3(a) is linearly polarized. Hence necessary modifications are required to design CP DRA which are explained in the next section. Generating CP waves requires essential stimulation of two orthogonal modes with a  $90^\circ$  angle difference between them [24]. In order to enhance the  $S_{11}$  bandwidth a bit more, and generate CP waves, a modification has been done in Figure 3(a) which leads the design to Figure 3(b).

**Generation of CP waves**

Antenna (b) is a traditional patch antenna, where a rectangular corner truncated-shaped aperture is introduced. These equal-sized rectangular corner truncated structures are placed in circular shapes with a uniform distance between them. It is basically a sequential rotation technique [25]. In addition to the microstrip feed line, the energy supply for the sequentially rotated patches is facilitated by using the gap-coupled feed method [26]. Moreover, to enhance the impedance and CP bandwidth, the four stacked patches are etched above the bottom layer. In the sequential rotation technique, the angular orientation of each element is adjusted to achieve the appropriate DR arrangement, resulting in the generation of CP waves [27].

To enhance the purity of CP, minimizing the cross-pol component of the total E-field of the array is crucial. This cross-pol

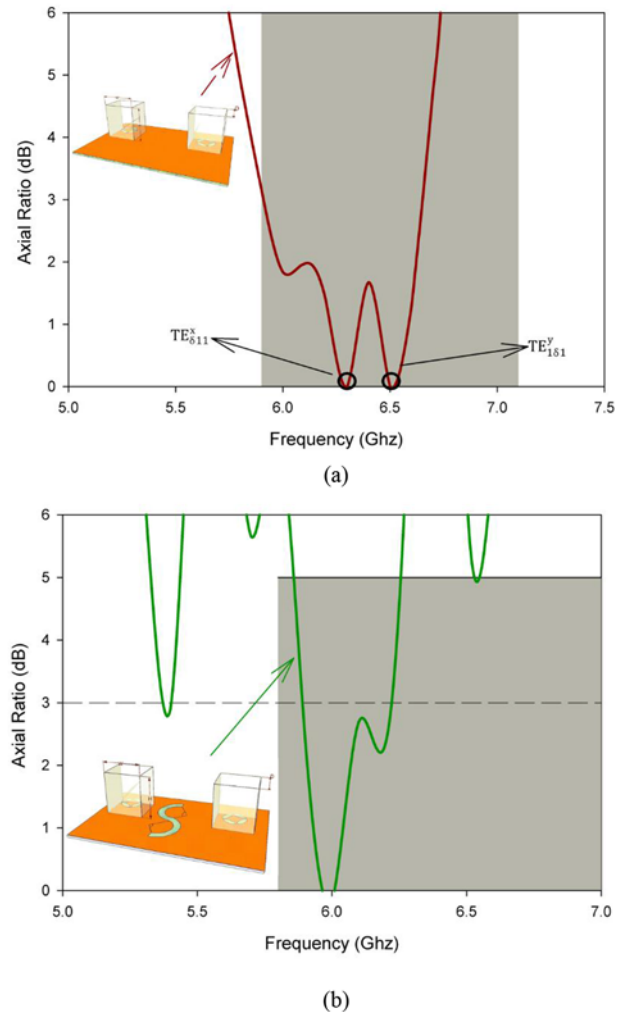


**Figure 6.** AR antenna evolution results (a) axial ratio antenna (a) and (b) axial ratio proposed design.

component is dependent on the microstrip feed line and the rotation angle of each array element with a circular shape aperture [28]. The best approach to reduce the cross-pol component is to apply a  $90^\circ$  rotation among the truncated structures and rotate each element in the quadruple array [29, 30]. In our specific case, as shown in Figure 2(c), each element has an angle  $\geq 90^\circ$  of spatial rotation, leading to the excitation of CP waves, resulting in the visibility of the degenerate modes pair of first higher-order in the DRs  $TE_{\delta 11}^x$  at 6.3 GHz and  $TE_{1\delta 1}^y$  at 6.49 GHz as depicted in Figure 6(a). On the other hand, CP response from the proposed antenna is almost a copy of antenna (b), i.e., 12.50 over the desired frequency band as depicted in Figure 6(b). The antenna modification provides a wide CP response over a bandwidth of approximately 13.20%, achieving an ARBW from 6.0 to 6.55 GHz, sufficiently covering the targeted band. The wideband CP response and excitation of higher-order modes have been accomplished using a low-cost, simple design configuration without any complexity, making a valuable contribution to the existing literature. Additionally, Figure 7 illustrates the E-field distribution of the proposed CP RDRA, providing evidence of the degenerate mode pair.

To gain deeper insights into reference antenna (b), Figure 8 displays the E-field vectors w.r.t angles in DRA-1 and DRA-2 at 6.3 GHz and 6.49 GHz, considering four different phases:

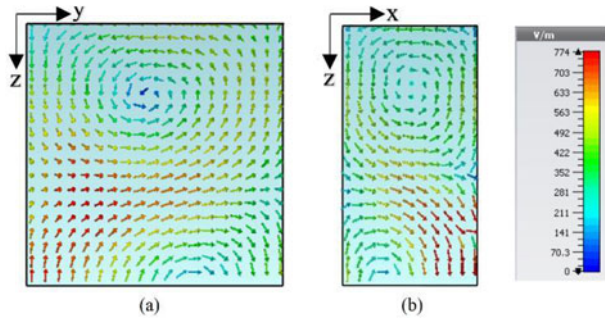


**Figure 7.** E-field distribution of the proposed circularly polarized RDRA: (a)  $TE_{\delta_{11}}^x$  excited at 6.3 GHz and (b)  $TE_{\delta_{11}}^y$  excited at 6.49 GHz.

Figure 8(a)  $0^\circ$ , Figure 8(b)  $90^\circ$ , Figure 8(c)  $180^\circ$ , and Figure 8(d)  $270^\circ$ .

In this analysis, DRA-1 is the only one excited, while DRA-2 remains receptive. As depicted in Figure 8, it is evident that the electric-field direction energized in operational DRA-1 undergoes a right-handed rotation as time progresses. The DRA-2 undergoes a counterclockwise rotation of its coupled electric field. Additionally, it is important to note that the wave propagation in DRA-1 occurs along the  $+y$  axis, whereas for other DR, it propagates toward the  $-y$  axis. As a result, the energized DRA-1 and the inactive DRA-2 exhibit LHCP electric fields.

Based on the above analysis, upon closer examination, it becomes evident that improving the port isolation could potentially be achieved by transforming the coupled electric field (E-field) in DRA-2 to RHCP radiation. This observation brings to light a promising method to enhance the isolation performance of the MIMO antenna.

### Mutual coupling suppression

High MC is undesirable in high-performance MIMO antennas, as depicted in the simulated results of both antenna (a) and antenna (b). The MC between antennas occurs through the propagation of surface waves or radiation [31]. Reducing radiation coupling can be achieved by increasing the gap between radiating elements, but this approach leads to an overall increase in the antenna's size. The MC performance  $S_{12}$  of antenna (a), antenna (b), and the proposed antenna is illustrated in Figure 4(d). It is evident that both antenna (a) and antenna (b) exhibit very high MC in the 5.5–6.3 GHz band, primarily attributed to the presence of surface waves at this lower frequency range. Now, to reduce surface wave coupling, a periodic S-shaped defect in the ground plane is created. The dimensions of the S-shaped slot and its position are selected in such a way that it creates a gap discontinuity for the 5.5–6.3 GHz band and the result is evident from the  $S_{12}$  of the proposed antenna. The significance of S-shaped defects in the ground plane can be known from the surface current distribution on the ground plane when one of the antenna elements is excited and another is kept passive. The transmission coefficient performance of the proposed antenna is shown in Figure 4(d). It can be clearly seen that the deep dip has been visible at 6.05 GHz this is due to the introduction of PDGS. Simulated results of MC suppression are well explained in the simulated results section.

Figure 9 shows the surface current distribution in the ground plane of the proposed antenna. It is clear that high MC is observed in Figure 9(a) while on the other hand, the current coupling from the active antenna element to the passive element is reduced by

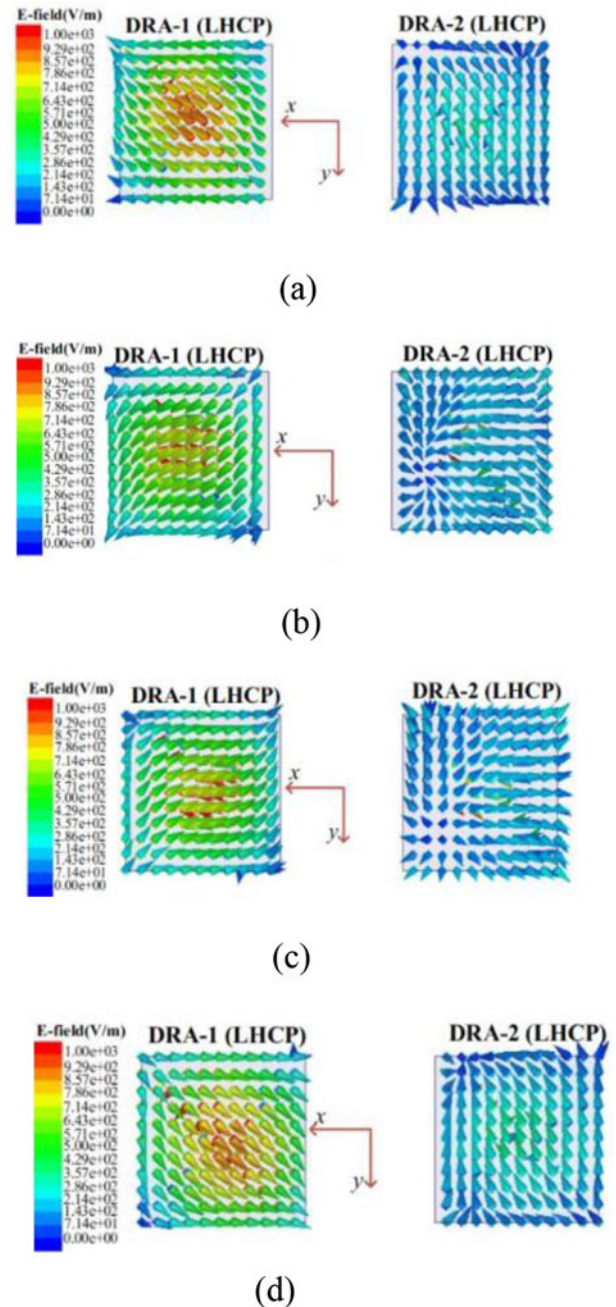


**Figure 8.** Simulated E-field vectors w.r.t. angles of reference antenna: (a)  $0^\circ$ , (b)  $90^\circ$ , (c)  $180^\circ$ , and (d)  $270^\circ$ .

the introduction of an S-shaped ground defect as illustrated in Figure 9(b).

### Measurement verification

To verify the design, a prototype of the proposed CP MIMO DRA was manufactured and subsequently subjected to testing. The fabrication process involved cutting two DRAs from a dielectric block with ECCOSTOCK HiK material having a  $\epsilon_r$  of 9.8. The energizing structure was realized by carving a printed circuit board made of F4BMX material. Figure 10 presents the prototype of the fabricated antenna. Figure 10(a)–(c) shows the aerial view and the underside perspective of the feeding structure, respectively.

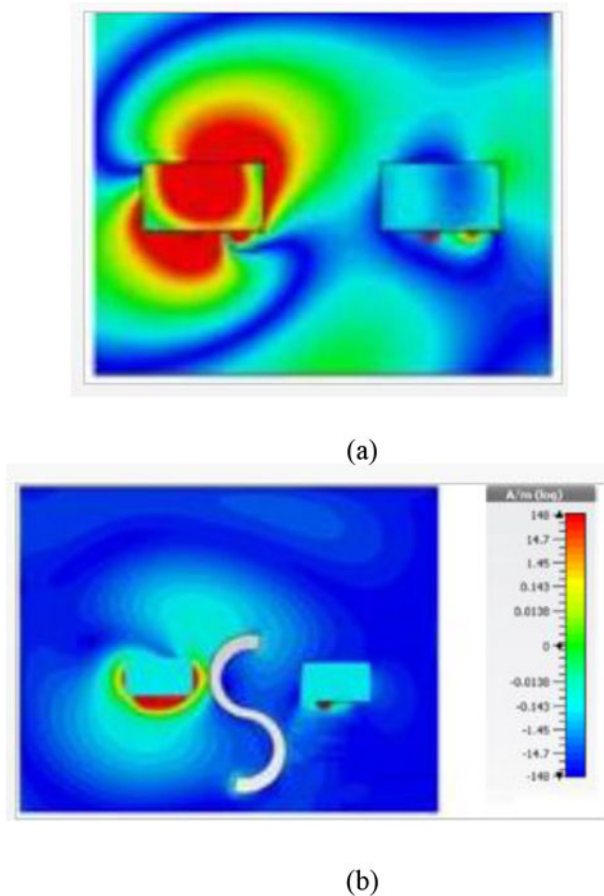


**Figure 9.** Current distributions of CP MIMO antenna at 6 GHz (a) with and (b) without DGS.

All dimensions of the prototype matched those shown in Figure 2(a)–(c). The measurement process closely followed the procedure used in [32]. To conduct a precise analysis, the S-parameters of the prototype were assessed by connecting the two ports of the DRAs to a Keysight E5071C vector network analyzer. Additionally, far-field parameters such as ARs, radiation patterns, and antenna gains were evaluated using a Satimo Starlab system, employing the traditional single-port method where one port is excited while the other is terminated with a matched load.

Simulated and measured results are shown in Figure 11. Moreover, in Figure 11(a) the prototype exhibited wide input IBWs, with simulated and measured values of approximately 35.10% (5.6–7.99 GHz) and 37.05% (5.5–8.0 GHz), respectively. A favorable agreement has been witnessed between the simulated and measured parameters. The measured IBW for both ports were determined to be  $\sim 36.30\%$  and  $\sim 36.10\%$ , respectively. Overall, there was a commendable correlation between the theoretical and experimental results, with minor discrepancies mainly attributed to limitations in the measurement process and fabrication errors. Furthermore, the isolation between the two feeding ports exhibited a negligible discrepancy, consistently staying better than  $-21$  dB across the operating band, as illustrated in Figure 11(b). While conducting the measurement process, one port of the antenna is actively stimulated, while the other port is connected to a 50-ohm matched load. Figure 11(c) depicts the AR

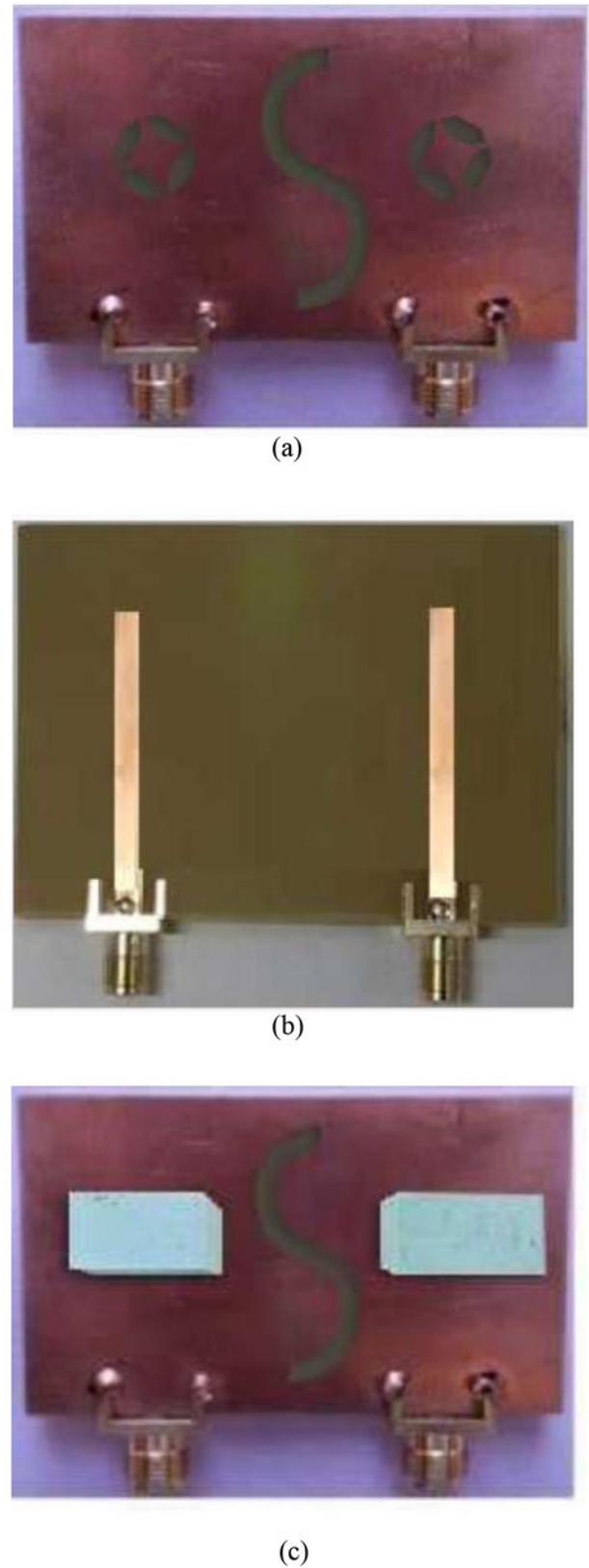


**Figure 10.** This figure showcases images of the constructed antenna: (a) provides a bottom view, (b) illustrates the feeding structure, and (c) displays the proposed antenna.

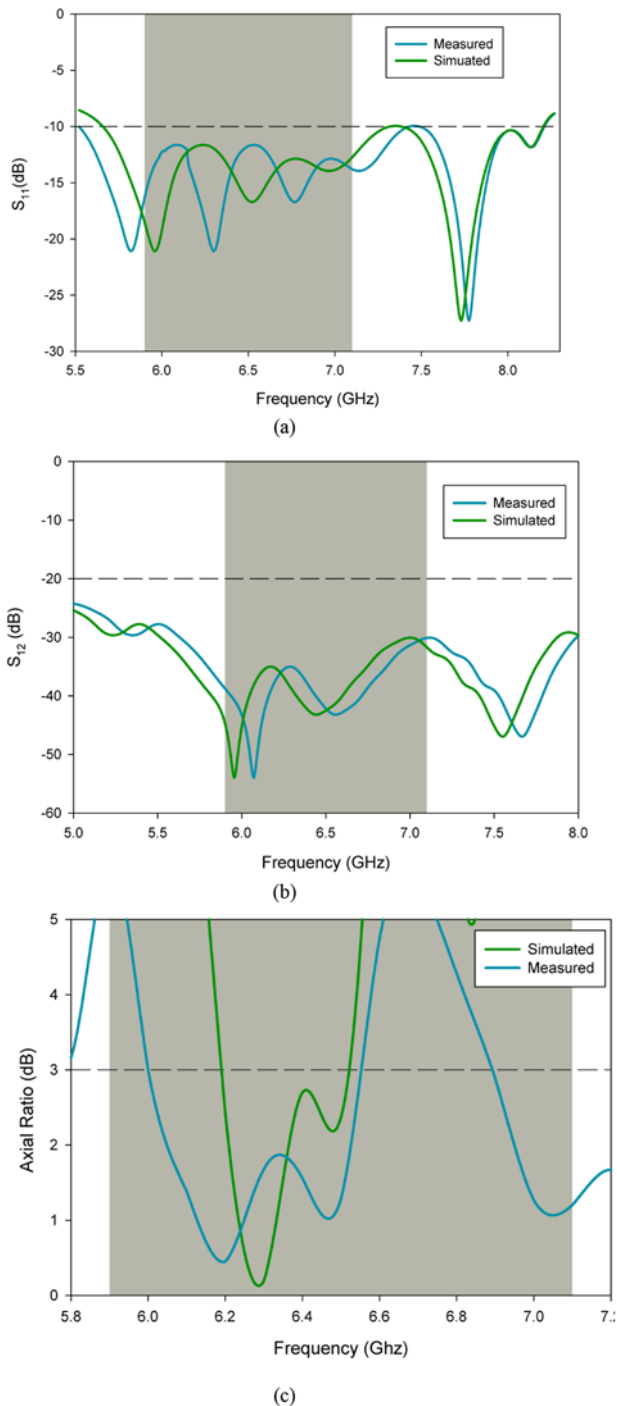


**Figure 11.** Tested and simulated outcomes of the two-port CP antenna in terms of (a)  $S_{11}$ , (b)  $S_{12}$ , and (c) 3-dB axial ratio.

in the broadside direction of the proposed model. The measured AR characteristics closely match the simulated ones, indicating a strong agreement between the two. Both the simulated and measured 3-dB ARBWs cover approximately 12.20% (from 6.0 to 6.55 GHz) and 10.07% (from 6.18 to 6.52 GHz), respectively. Furthermore, the experimental return loss ( $S_{11}$ ) and CP (3-dB) bandwidths exhibit significant overlap, providing consistency and validation of the antenna's performance. The combined ARBW and IBW cover the frequency range suitable for the Wi-Fi 6E band,

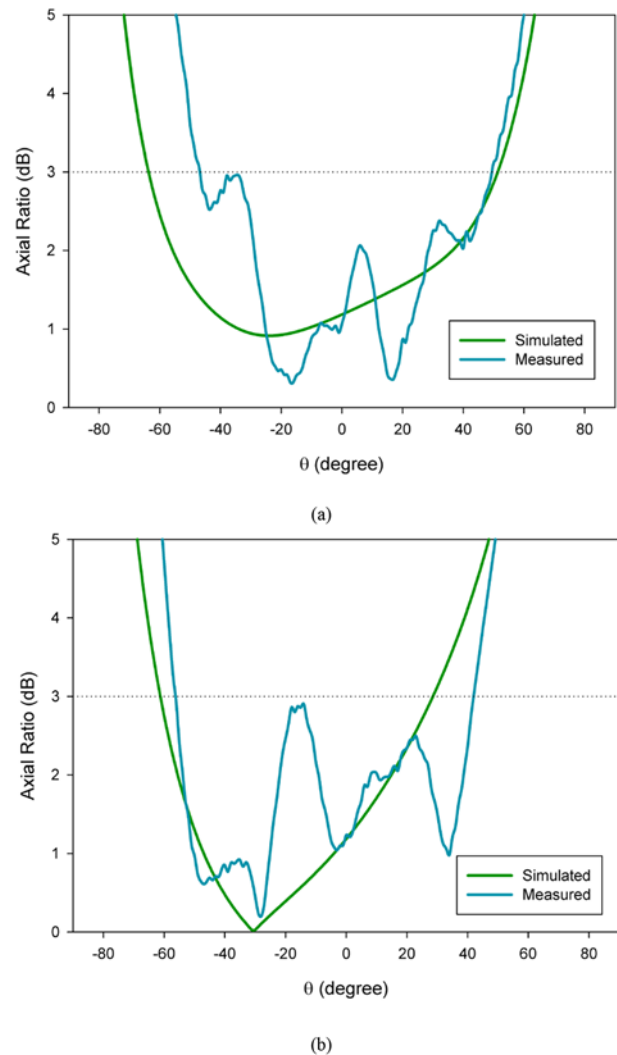


**Figure 12.** Results of MIMO antenna at 7 GHz in terms of (a) beamwidth at  $\Theta = 0^\circ$  and (b) beamwidth at  $\Theta = 90^\circ$ .

showcasing the suitability of the proposed antenna for applications within this band.

To demonstrate the CP characteristics of the MIMO antenna, Figure 12(a) and (b) illustrates the 3-dB ARBWs are measured to be  $110^\circ$  and  $95^\circ$  along the XZ and YZ planes, respectively. The boresight AR is recorded at 0.86 dB. These findings highlight the antenna's ability to maintain CP over specific beam widths in both planes, further affirming its suitability for MIMO applications.

The radiation patterns, both measured and simulated, at  $\phi = 0^\circ$  and  $\phi = 90^\circ$  planes for two ports at 7 GHz are depicted in Figure 13. Notably, in the direction of the boresight, the LHCP field is stronger than the RHCP field by more than 13 dB, in comparison to the cross-polar fields (right-hand CP). This substantial disparity between the co-polar and cross-polar fields, deemed to be of paramount importance for a diverse array of practical applications, underscores the efficacy and suitability of the antenna design. The same geometry (spatial diversity) concept and phenomena for LHCP of radiation patterns have been discussed in [38]. Although there is a slight variation in the radiation patterns when the elementary antenna is configured as an MIMO antenna, this variation is mainly attributed to the presence of an additional substrate and other antenna elements in close proximity.



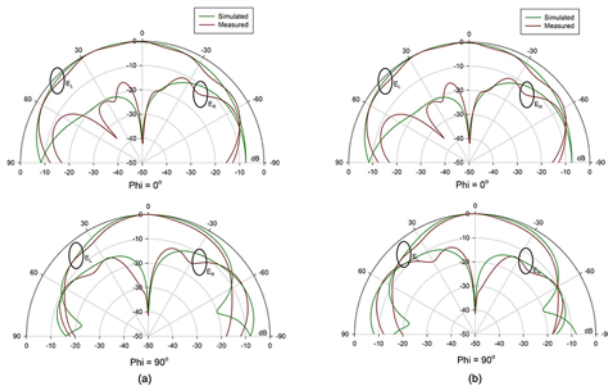


**Figure 13.** Radiation patterns of the proposed CP MIMO DRA at 7 GHz. (a) Port 1. (b) Port 2.

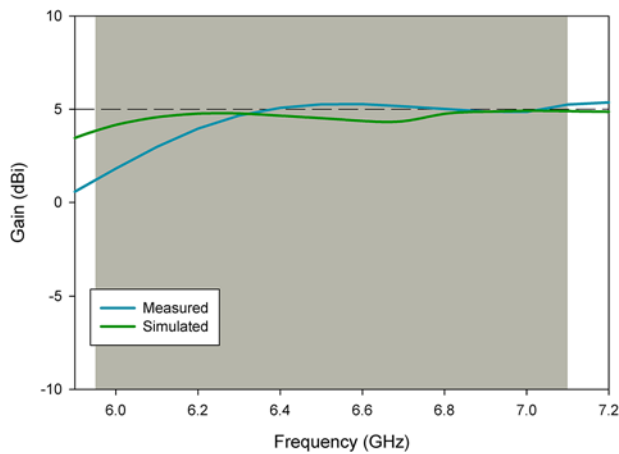


**Figure 14.** Tested and simulated gain.

Nevertheless, even with the MIMO configuration, the overall shape of the radiation patterns remains almost identical to that of the elementary antenna. The measurement of these patterns is carried out in an automatic anechoic chamber, ensuring a controlled and isolated environment for precise characterization of the antenna’s performance. Figure 14 illustrates the gain of the suggested configuration, showcasing a mean measured gain of 5.01 dBic. The measured gain is slightly less which could be due to fabrication and measurement setup inaccuracies.

**MIMO diversity analysis**

The performance and capabilities of the MIMO antenna are validated using the ECC and diversity gain. In an ideal scenario, ECC should be 0 [33]; however, a practical limit for better ECC is typically considered to be <0.5. ECC is a crucial parameter used to assess the similarity of received signals, indicating the level of MC. Its value ranges from 0 to 1. For the measurements conducted in an outdoor setting, the ECC results are remarkably promising, with values consistently below 0.01, well within the safe threshold [34]. Figure 15 illustrates the ECC of the CP MIMO antenna parameters, where the ECC for Port 1 and Port 2 is computed using far-field radiation patterns with Equation (1). The measured ECC for the proposed wideband CP MIMO antenna is consistently below 0.04 for the entire operating band. These findings

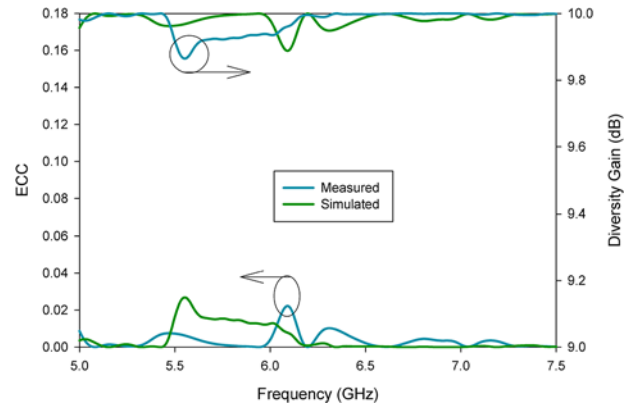


**Figure 15.** ECC of CP MIMO antenna parameters.

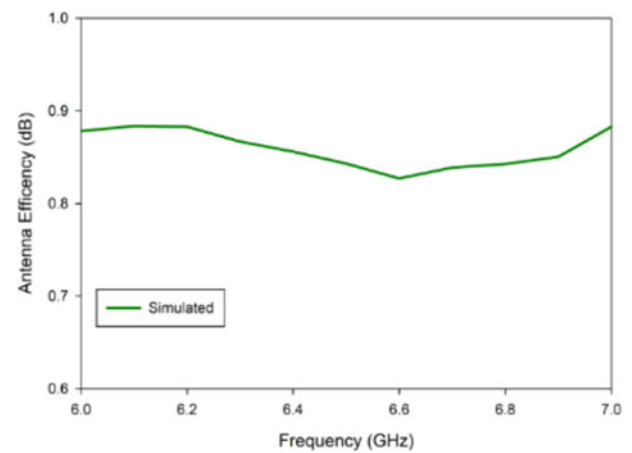


**Figure 16.** Antenna efficiency of the proposed circularly polarized MIMO DRA.

further emphasize the antenna’s effectiveness in reducing MC and ensuring reliable performance. Diversity gain serves as an important metric for assessing the efficacy of MIMO antenna systems. In an ideal scenario, a DG value of 10 is desirable, but in practical terms, a value exceeding 6 is typically considered satisfactory [35]. As depicted in Figure 15, the measured diversity gain for the newly designed wideband CP-MIMO antenna surpasses 8 dB. The following formula can be employed to compute the diversity gain of the MIMO antenna. Along with this the antenna efficiency of the proposed antenna is illustrated in Figure 16, revealing a consistent efficiency of approximately 90 % within the desired frequency band. This achievement underscores the robustness and effectiveness of the antenna design in converting input power into radiated energy, thus affirming its suitability for practical applications.

$$\rho_e = \frac{4\pi F_1(\theta, \phi) \cdot F_2(\theta, \phi) d\Omega}{24\pi F_1(\theta, \phi)^2 d\Omega + 4\pi F_2(\theta, \phi)^2 d\Omega} \tag{1}$$

$$DG = 10\sqrt{1 - \rho_e^2} \tag{2}$$

Table 2 presents a comprehensive evaluation of the performance of the proposed CP MIMO antenna system in comparison to other existing CP MIMO systems. The assessment encompasses various factors, including size, operating bandwidth, ARBW, isolation, and

**Table 2.** Augmented dimension of the projected wideband CP MIMO antenna

Lit.	Size (mm <sup>2</sup> )/ Num. of ports	Resonant freq (GHz)	S <sub>11</sub> %	Axial ratio %	Separation (dB)	ECC	Design
[8]	41 × 51/2	5.73	18.81% (5.23–6.03)	4.47% (5.72–5.94)	24	0.08	DRA
[9]	86.7 × 16.6	3.63	22.3% (3.26–4.00)	5.77% (3.7–3.56)	21	<0.02	DRA
[10]	57 × 33/2	5.6	24.83 (5.3–6.7)	14.78% (5.20–5.96)	21	<0.6	Planar structure
[11]	160 × 110/2	2.6	3.3% (2.58–2.66)	6.20% (2.50–2.66)	20	0.003	Planar structure
[12]	37 × 30/2	3.86	25% (3.4–4.3)	25% (3.4–4.3)	>16	<0.11	Planar structure
[14]	50 × 50/4	12	10.18% (11.6–12.6)	9.88% (11.8–12.9)	>21	Nil	Metamaterial multilayer
[39]	53 × 54/4	6	65.01% (3.81–7.48)	20.10% (5.47–6.70)	>15	<0.01	Planar
[15]	45.6 × 45.6/4	7.92/11.12	6.90% (7.69–12.6) & 16.7% (9.34–11.88)	6.6% (9.75–10.41)	20	<0.03	Multilayer
<b>This work</b>	<b>53 × 53/2</b>	<b>7</b>	<b>37.10% (5.5–8.0)</b>	<b>12.20% (6.0–6.55)</b>	<b>&gt;21</b>	<b>&lt;0.02</b>	<b>DRA</b>

ECC. The proposed antenna demonstrates notable strengths, particularly in terms of size, operating bandwidth, and ARBW. With its DRA structure, it achieves a wide overlapping impedance and ARBW, effectively covering the Wi-Fi 6E band. Additionally, the antenna exhibits outstanding ECC, further enhancing its suitability for MIMO applications. In direct comparison to state-of-the-art CP MIMO antennas, the suggested antenna stands out as a compelling option due to its superior performance across the evaluated parameters.

## Conclusion

In this study, a two-port wideband CP antenna employing simple geometry and DRA structure is analyzed. The CP is achieved through the utilization of rectangular-shaped truncated slots, positioned orthogonally on the ground plane. To mitigate MC, an S-shaped DGS is incorporated. The MIMO antenna's physical dimensions are 53 × 53 × 1.6 mm<sup>3</sup>, enabling coverage of the Wi-Fi 6E band (5.91–7.10 GHz) and delivering a respectable gain of ~5.10 dBic across the frequency range. The radiation patterns resemble dipoles and are consistently observed for both individual and MIMO antennas along the XZ and YZ planes. To assess the MIMO performance, the antenna is evaluated in terms of ECC and diversity gain. The results indicate that the antenna's MIMO performance falls within acceptable limits, demonstrating its suitability for Wi-Fi 6E applications in the future. In conclusion, the proposed two-port CP MIMO antenna showcases distinctive advantages, such as CP, favorable radiation characteristics, and a DRA-based design. These attributes position it as a promising option for forthcoming Wi-Fi 6E implementations.

**Acknowledgements.** The authors would like to thank King Saud University for supporting this research by Researcher's Supporting Project (RSP2024R71).

**Author contributions.** J.I. and U.I. designed the proposed model and M.R. and I.S. performed the simulations and fabrication. All authors contributed equally to analyzing data and reaching conclusions, answering the review, and writing the paper.

**Competing interests.** The authors report no conflict of interest.

## References

- Pan S, Lin M, Ming X, Zhu S, Bian L-A and Gaosheng L (2021) A low-profile programmable beam scanning holographic array antenna without phase shifters. *IEEE Internet of Things Journal* **9**(11), 8838–8851.
- Li A, Masouros C, Swindlehurst AL and Yu W (2021) 1-Bit massive MIMO transmission: Embracing interference with symbol-level precoding. *IEEE Communications Magazine* **59**, 121–127.
- Li B, Zhang M, Rong Y and Han Z (2022) Transceiver optimization for wireless powered time-division duplex MU-MIMO systems: Non-robust and robust designs. *IEEE Transactions on Wireless Communications* **21**, 4594–4607.
- Nasir J, Jamaluddin MH, Khalily M, Kamarudin MR and Ullah I (2016) Design of an MIMO dielectric resonator antenna for 4G applications. *Wireless Personal Communications* **88**, 525–536.
- Nadeem I and Choi D-Y (2018) Study on mutual coupling reduction technique for MIMO antennas. *IEEE Access* **7**, 563–586.
- Jamal MY, Li M and Jiang L (2020) A novel planar dual CP MIMO antenna with polarization diversity and high isolation. In *2020 IEEE International Symposium on Antennas and Propagation and North American Radio Science Meeting*, pp. 1927–1928.
- Li B, Zhang M, Rong Y and Han Z (2021) Transceiver optimization for wireless powered time-division duplex MU-MIMO systems: Non-robust and robust designs. *IEEE Transactions on Wireless Communications* **21**, 4594–4607.
- Das G, Sharma A and Gangwar RK (2018) Dielectric resonator based circularly polarized MIMO antenna with polarization diversity. *Microwave and Optical Technology Letters* **60**, 685–693.
- Singhwal S, Kanaujia B, Singh A, Kishor J and Matekovits L (2020) Multiple input multiple output dielectric resonator antenna with circular polarized adaptability for 5G applications. *Journal of Electromagnetic Waves and Applications* **34**, 1180–1194.
- Tran HH, Hussain N and Le TT (2019) Low-profile wideband circularly polarized MIMO antenna with polarization diversity for WLAN applications. *AEU-International Journal of Electronics and Communications* **108**, 172–180.
- Jamal MY, Li M and Yeung KL (2020) Isolation enhancement of closely packed dual circularly polarized MIMO antenna using hybrid technique. *IEEE Access* **8**, 11241–11247.
- Dwivedi AK, Sharma A, Pandey AK and Singh V (2021) Two port circularly polarized MIMO antenna design and investigation for 5G communication systems. *Wireless Personal Communications* **120**, 2085–2099.

13. **Illahi U, Iqbal J, Ismail Sulaiman M, Alam M, Mohd Su'ud M and Khattak MI** (2020) Design and development of a singly-fed circularly polarized rectangular dielectric resonator antenna for WiMAX/Satellite/5G NR band applications. *AEU-International Journal of Electronics and Communications* **126**, 153443.
14. **Kumar A and Agrawal T** (2021) High performance circularly polarized MIMO antenna with polarization independent metamaterial. *Wireless Personal Communications* **116**, 3205–3216.
15. **Eslami A, Nourinia J, Ghobadi C and Shokri M** (2021) Four-element MIMO antenna for X-band applications. *International Journal of Microwave and Wireless Technologies* **13**, 859–866.
16. **Khalid M, Naqvi SI, Hussain N, Rahman M, Fawad SSM, Khan MJ and Amin Y** (2020) 4-Port MIMO antenna with defected ground structure for 5G millimeter wave applications. *Electronics* **9**(1), 71.
17. **Xu K-D, Guo Y-J, Liu Y, Deng X, Chen Q and Zhewang M** (2021) 60-GHz compact dual-mode on-chip bandpass filter using GaAs technology. *IEEE Electron Device Letters* **42**(8), 1120–1123.
18. **Kollipara V and Peddakrishna S** (2022) Quad-port circularly polarized MIMO antenna with wide axial ratio. *Sensors* **22**, 7972.
19. **Fang X, Leung K, Lim E and Chen R** (2010) Compact differential rectangular dielectric resonator antenna. *IEEE Antennas and Wireless Propagation Letters* **9**, 662–665.
20. **Long R, Dorris R, Long S, Khayat M and Williams J** (2001) Use of parasitic strip to produce circular polarisation and increased bandwidth for cylindrical dielectric resonator antenna. *Electronics Letters* **37**, 1.
21. **Leung KW and Ng HK** (2003) Theory and experiment of circularly polarized dielectric resonator antenna with a parasitic patch. *IEEE Transactions on Antennas and Propagation* **51**, 405–412.
22. **Leung KW** (2000) Conformal strip excitation of dielectric resonator antenna. *IEEE Transactions on Antennas and Propagation* **48**, 961–967.
23. **Ding K, Hong R, Guan D, Liu L and Wu Y** (2020) Broadband circularly polarised stacked antenna with sequential-phase feed technique. *IET Microwaves, Antennas & Propagation* **14**, 779–784.
24. **Yun S, Kim D-Y and Nam S** (2012) Bandwidth enhancement of cavity-backed slot antenna using a via-hole above the slot. *IEEE Antennas and Wireless Propagation Letters* **11**, 1092–1095.
25. **Li R, DeJean G, Laskar J and Tentzeris MM** (2005) Investigation of circularly polarized loop antennas with a parasitic element for bandwidth enhancement. *IEEE Transactions on Antennas and Propagation* **53**, 3930–3939.
26. **Sulaiman MI and Khamas SK** (2011) A singly fed wideband circularly polarized dielectric resonator antenna using concentric open half-loops. *IEEE Antennas and Wireless Propagation Letters* **10**, 1305–1308.
27. **Abedian M, Rahim S, Danesh S, Jamaluddin M and Islam M** (2017) Compact wideband circularly polarised dielectric resonator antenna. *Electronics Letters* **53**, 5–6.
28. Manual (2002) C. M. S. CST Darmstadt, Germany.
29. **Li B and Leung KW** (2005) Strip-fed rectangular dielectric resonator antennas with/without a parasitic patch. *IEEE Transactions on Antennas and Propagation* **53**, 2200–2207.
30. **Lim EH, Leung KW and Fang X** (2010) The compact circularly-polarized hollow rectangular dielectric resonator antenna with an underlaid quadrature coupler. *IEEE Transactions on Antennas and Propagation* **59**, 288–293.
31. **Iqbal J, Illahi U, Sulaiman MI, Alam MM, Su'ud MM and Yasin MNM** (2019) Mutual coupling reduction using hybrid technique in wideband circularly polarized MIMO antenna for WiMAX applications. *IEEE Access* **7**, 40951–40958.
32. **Fang X, Leung KW and Lim EH** (2014) Singly-fed dual-band circularly polarized dielectric resonator antenna. *IEEE Antennas and Wireless Propagation Letters* **13**, 995–998.
33. **Mongia RK** (1992) Theoretical and experimental resonant frequencies of rectangular dielectric resonators. In *IEE Proceedings H (Microwaves, Antennas and Propagation)* Vol. 139, IET Digital Library, pp. 98–104.
34. **Abdulmajid AA, Khalil Y and Khamas S** (2018) Higher-order-mode circularly polarized two-layer rectangular dielectric resonator antenna. *IEEE Antennas and Wireless Propagation Letters* **17**, 1114–1117.
35. **Hu Y, Pan YM and Di Yang M** (2021) Circularly polarized MIMO dielectric resonator antenna with reduced mutual coupling. *IEEE Transactions on Antennas and Propagation* **69**, 3811–3820.
36. **Alieldin A, Huang Y, Stanley M, Joseph SD and Lei D** (2018) A 5G MIMO antenna for broadcast and traffic communication topologies based on pseudo inverse synthesis. *IEEE Access* **6**, 65935–65944.
37. **Huang H, Li X and Liu Y** (2018) 5G MIMO antenna based on vector synthetic mechanism. *IEEE Antennas and Wireless Propagation Letters* **17**, 1052–1055.
38. **Chen H-D, Kulkarni J, Lo J-J and Hsuan Y-C** (2021) Recent designs to achieving wideband MIMO antenna for 5G NR sub-6GHz smartphone applications. In *2020 International Symposium on Antennas and Propagation (ISAP)*, IEEE, 417–418.
39. **Yousef BM, Ameen AM, Desai A, Hsu H-T, Dhasarathan V and Ibrahim AA** (2023) Defected ground structure-based wideband circularly polarized 4-port MIMO antenna for future Wi-Fi 6E applications. *AEU-International Journal of Electronics and Communications* **170**, 154815.



**Dr. Javed Iqbal** holds a B.Sc. degree in Telecommunication Engineering from N.W.F.P. University of Engineering & Technology, Peshawar, Pakistan (2007), an M.S. degree in Electronic Communication and Computer Engineering from the University of Nottingham, Malaysia campus (2013), and a Ph.D. in Electrical and Electronic Engineering from Universiti Kuala Lumpur, Gombak, Malaysia (2019). Currently

serving as the Head of the Department and Assistant Professor in the Faculty of Engineering and Technology at Gomal University, Pakistan. Dr. Iqbal conducted research fellowship at Universiti Sains Malaysia from 2021 to 2022. His research focuses on circularly polarized MIMO dielectric resonator antennas, 5G NR band applications, millimeter waves, and wireless body area networks (WBANs). Dr. Javed Iqbal has received accolades such as the Best Paper of the Year in 2019 from IEEE Malaysia Chapter and the ANUGERAH SANGGAR SANJUNG USM 2021 award for a high-impact factor journal publication in 2022. He is also a member of professional societies and holds registrations as a graduate engineer and registered engineer in Malaysia and Pakistan, respectively. Additionally, he is an approved Ph.D. supervisor by the Higher Education Commission of Pakistan.



**Dr. Usman Illahi** received a B.Sc. degree in Electrical Engineering from the NWFP University of Engineering and Technology, Peshawar, Pakistan, in 2007, an M.Sc. degree in Electronic Communication and Computer Engineering from the University of Nottingham Malaysia, in 2013, and a Ph.D. degree in Electrical and Electronic Engineering from Universiti Kuala Lumpur, Malaysia, in 2019, with a focus on RF and

microwave communication systems and especially antennas, such as dielectric resonator antennas, circularly polarized antennas, wideband antennas, MIMO antennas, wearable antennas, ML in antennas, and antennas for 5G/6G communication systems. He has authored many impact factor journals and peer-reviewed conferences. He is a reviewer of many prestigious journals in the field of engineering and technology.



**Dr. Shahid M. Ramay** is currently an Associate Professor in the Department of Physics and Astronomy, King Saud University, Riyadh, Saudi Arabia. He received his M.Phil. degree from Quaid-i-Azam University Islamabad and Ph.D. from Center of Excellence in Solid State Physics, Punjab University Lahore, Pakistan. His main research area is ferrimagnetic materials and studied their magnetic and dielectric properties at low and high temperatures. Currently he is also

working on Energy Storage Materials with Density Functional theory and Electrochemical way. He has published more than 200 articles in impact factor journals.



**Dr. Mohamad Ismail Sulaiman** Mohamad Ismail Sulaiman received the M.Eng. and Ph.D. degrees in electronic engineering (communications) from the University of Sheffield, U.K., in 2012 and 2007, respectively. Since 2013, Now he has been working as Tutor in the University of Sheffield International College, he was a Senior Lecturer at the Universiti Kuala Lumpur British Malaysian Institute. He has authored more than 30 research articles published in journals and peer-reviewed conferences. His research interests include computational electro-

magnetic, dielectric resonator antennas, circularly polarized antennas, wide-band antennas, mutual coupling, MIMO antennas, and wearable antennas.